Dong *et al. Genes & Nutrition* (2024) 19:17
https://doi.org/10.1186/s12263-024-00754-5

Genes & Nutrition

RESEARCH Open Access

Protective effects of Nogo-B deficiency in NAFLD mice and its multiomics analysis of gut microbiology and metabolism

Xu Dong[1,2,3†], Yu-Ting Xiong[4†], Tingting He[5†], Congyang Zheng[1,2,3], Junjie Li[3,7], Yingjie Zhuang[2], Yingjie Xu[3], Ye Xiu[3], Zhixin Wu[3], Xiaomei Zhao[3], Xiaohe Xiao[3,6*], Zhaofang Bai[3,6*] and Lili Gao[1,2*]

Abstract

Background Nonalcoholic fatty liver disease (NAFLD) is a prevalent chronic liver ailment that can lead to serious conditions such as cirrhosis and hepatocellular carcinoma. Hepatic Nogo-B regulates glucose and lipid metabolism, and its inhibition has been shown to be protective against metabolic syndrome. Increasing evidence suggests that imbalances in the gut microbiota (GM) and lipid metabolism disorders are significant contributors to NAFLD progression. Nevertheless, it is not yet known whether Nogo-B can affect NAFLD by influencing the gut microbiota and metabolites. Hence, the aim of the present study was to characterize this process and explore its possible underlying mechanisms.

Methods A NAFLD model was constructed by administering a high-fat diet (HFD) to Nogo-B$^{-/-}$ and WT mice from the same litter, and body weight was measured weekly in each group. The glucose tolerance test (GTT) and insulin tolerance test (ITT) were performed to assess blood glucose levels. At the end of the 12-week period, samples of serum, liver, and intestinal contents were collected and used for serum biochemical marker and inflammatory factor detection; pathology evaluation; and gut microbiome and metabolomics analysis. Spearman's correlation analysis was performed to determine possible correlations between differential gut microbiota and differential serum metabolites between groups.

Results Nogo-B deficiency attenuated the effects of the HFD, including weight gain, liver weight gain, impaired glucose tolerance, hepatic steatosis, elevated serum lipid biochemicals levels, and liver function. Nogo-B deficiency suppressed M1 polarization and promoted M2 polarization, thus inhibiting inflammatory responses. Furthermore, Nogo-B$^{-/-}$-HFD-fed mice presented increased gut microbiota richness and diversity, decreased *Firmicutes/Bacteroidota* (F/B) ratios, and altered serum metabolites compared with those of WT-HFD-fed mice. During analysis,

†Xu Dong, Yu-Ting Xiong and Tingting He contributed equally to this work.

*Correspondence:
Xiaohe Xiao
pharmacy_302@126.com
Zhaofang Bai
baizf2008@hotmail.com
Lili Gao
gll301818@163.com

Full list of author information is available at the end of the article

several differential gut microbiota, including *Lachnoclostridium*, *Harryflintia*, *Odoribacter*, *UCG-009*, and *unclassified_f_Butyricoccaceae*, were screened between groups. These microbiota were found to be positively correlated with upregulated purine metabolism and bile acid metabolites in Nogo-B deficiency, while they were negatively correlated with downregulated corticosterone and tricarboxylic acid cyclic metabolites in Nogo-B deficiency.

Conclusion Nogo-B deficiency delayed NAFLD progression, as demonstrated by reduced hepatocellular lipid accumulation, attenuated inflammation and liver injury, and ameliorated gut microbiota dysbiosis and metabolic disorders. Importantly, *Odoribacter* was strongly positively correlated with ALB and taurodeoxycholic acid, suggesting that it played a considerable role in the influence of Nogo-B on the progression of NAFLD, a specific feature of NAFLD in Nogo-B$^{-/-}$ mice. The regulation of bile acid metabolism by the gut microbiota may be a potential target for Nogo-B deficiency to ameliorate NAFLD.

Keywords NAFLD, Nogo-B, Gut microbiota, Metabonomics

Introduction

With a high global prevalence of 32%, nonalcoholic fatty liver disease (NAFLD) has become the most common chronic liver disease and the primary cause of cirrhosis and hepatocellular carcinoma (HCC) [1, 2]. NAFLD is a metabolic stress-induced liver injury that is closely linked to insulin resistance (IR) and genetic susceptibility, encompassing a spectrum of diseases ranging from steatosis to nonalcoholic steatohepatitis (NASH), cirrhosis, and even HCC [3].

Moreover, NAFLD is bidirectionally associated with metabolic syndromes such as obesity, IR, hypertension, hyperlipidemia, and hyperglycemia, and up to 80% of obese patients and 65.04% of diabetic patients can be complicated with NAFLD [4, 5].

Mechanically, hepatic steatosis and related inflammation caused by excessive lipid deposition are important mechanisms for the development of NAFLD [6]. Excess lipid deposition and metabolic disorders lead to lipotoxic lipid formation, which leads to cellular oxidative stress, endoplasmic reticulum stress, inflammasome activation, and apoptotic cell death and subsequently triggers inflammation, fibrogenesis and tissue regeneration [7, 8]. In addition, the mechanism of the occurrence and progression of NAFLD is influenced by metabolic, genetic and microbial factors [3, 9].

The gut microbiota (GM) is a novel organ that plays a crucial role in NAFLD pathophysiology [10]. Specifically, a previous study revealed that a dysbiotic microbiome, which is considered one of the primary risk factors for NAFLD, is frequently observed among obese individuals [11]. Furthermore, alterations in the composition of the GM are commonly observed in patients with NAFLD, and even microbiome signatures are associated with advanced fibrosis [12, 13]. Moreover, the influence of the GM on NAFLD is inseparable from metabolism, and the gut–liver axis plays a vital role in metabolic diseases [10]. A study demonstrated a disruption of bile acid profiles in the serum and stool of patients with NASH due to reduced microbial diversity and loss of members of the GM responsible for the production of secondary bile acids [14]. Thus, microbes, metabolism, and their interactions affect the disease progression of NAFLD, and the role of the microbiome in metabolic disorders has gained increased attention.

Nogo proteins containing Nogo-A, Nogo-B, and Nogo-C splice variants belong to the reticulon protein family, which are expressed mainly on the cell surface and in the endoplasmic reticulum (ER) [15, 16]. Each Nogo protein splice variant is tissue-dependent, and Nogo-B is the only detectable member in the liver and circulation. Nogo-B is enriched in most tissues, including the liver, kidney, lung, nerve, and blood vessels, and in inflammatory cells, such as bone marrow-derived macrophages (BMDMs) and human monocytes (CD14+) [17]. Recently, a growing number of studies have revealed that the Nogo-B protein is strongly expressed in activated macrophages and may have broader effects on the polarization and recruitment of macrophages, potentially contributing to inflammatory processes [18, 19]. Yuan Tian et al. demonstrated that Nogo-B regulates metabolic reprogramming of oxidation-modified low-density lipoproteins (oxLDLs) through the CD36-Nogo-B-YAP pathway, facilitating the progression of hepatitis to HCC [20]. Moreover, Nogo-B deficiency can effectively ameliorate liver injury and fibrosis exacerbated by PPARγ deficiency by inhibiting hepatic stellate cell activation, TLR4-NFκB/TNF-α signaling, and M1 macrophage polarization [21]. Thus, Nogo-B protein plays a nonnegligible role in liver disease progression.

Currently, research on the relationships between Nogo-B and NAFLD in the gut–liver axis and the GM and its metabolites is limited. Thus, in the present study, we established a high-fat diet-induced NAFLD model using Nogo-B knockout (KO) mice to identify the impact of Nogo-B on the gut microbiota and metabolites in NAFLD. We also performed a correlation analysis to reveal the associations between differential communities and metabolites.

Methods

Animals

The overall experimental design is shown in Fig. 1. Wild-type (WT) mice, Nogo-B$^{-/-}$ mice, and Nogo-B$^{+/-}$ mice were C57BL/6J male mice housed in the SPF-grade Laboratory Animal Center of Beijing Biocytogen Co., Ltd. (Beijing, China). The Nogo-B$^{-/-}$ mice used in this study were previously generated via CRISPR/Cas9 technology [22]. According to the first exon base sequence of Nogo-B gene, sgRNA targeting Nogo-B was designed, sgRNA expression plasmid was constructed, and sgRNA and Cas9 mRNA were transcribed in vitro for microinjection into the fertilized eggs of C57BL/6 mice. Gene sequencing was used to detect the mutation of Nogo-B gene base, total protein was extracted from mouse liver homogenate, and the expression of Nogo-B in liver was detected by Western Blot, thus confirming the successful knockout of Nogo-B gene. Compared with wild-type mice, Nogo-B knockout mice presented no significant differences in liver function indices (aminotransferases, bilirubin, albumin and alkaline phosphatase). To obtain WT mice and Nogo-B$^{-/-}$ mice from the same litter and of the same age, hybridization was performed on the Nogo-B$^{+/-}$ mice, followed by tail genotype identification and screening using

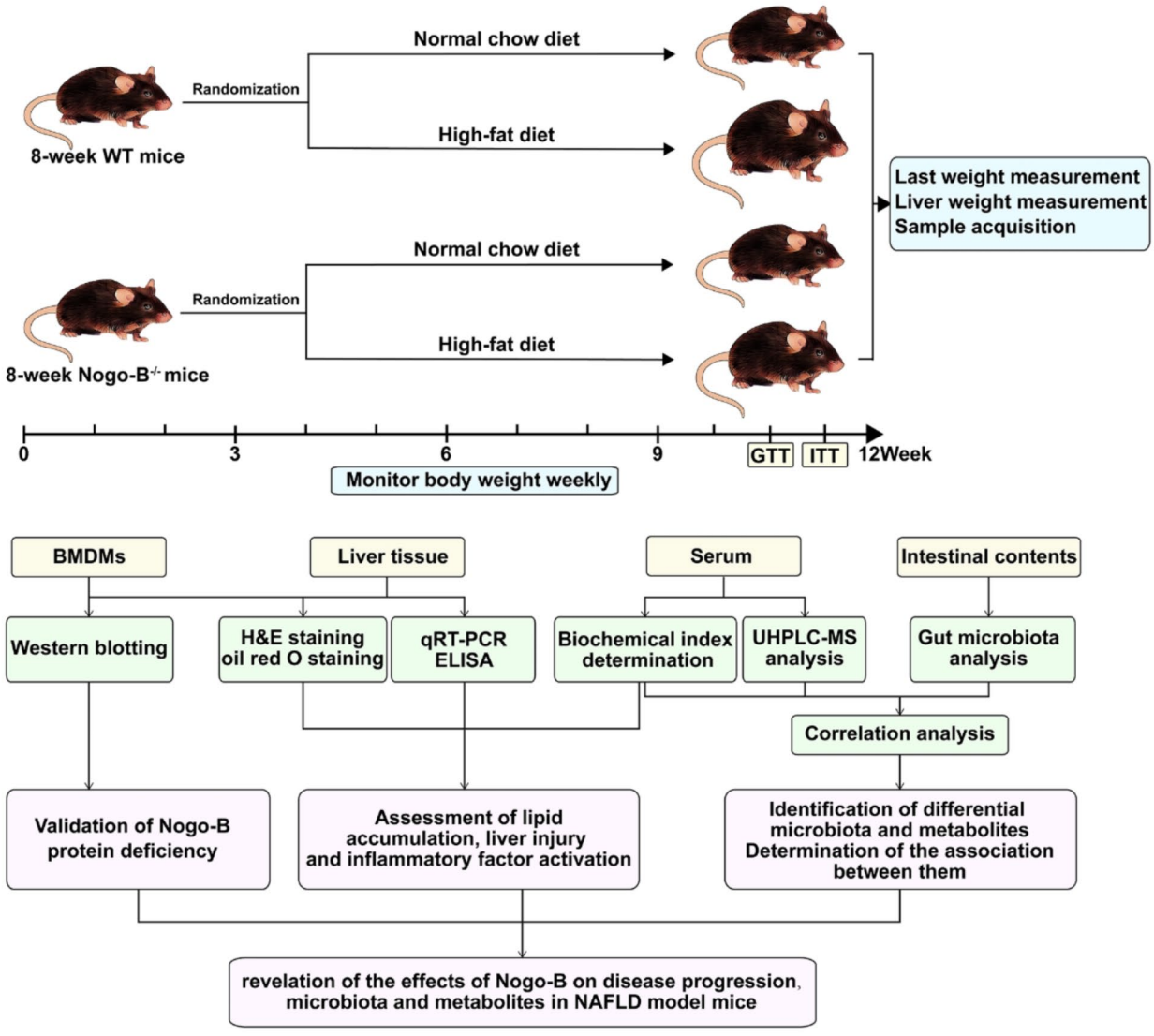

Fig. 1 Flow chart of the experiment. WT, wild-type; GTT, glucose tolerance test; ITT, insulin tolerance test; BMDMs, bone marrow-derived macrophages; H&E, hematoxylin and eosin; qRT–PCR, quantitative real-time polymerase chain reaction; ELISA, enzyme-linked immunosorbent assay; NAFLD, nonalcoholic fatty liver disease

the primer sequences listed in supplementary material Table S1.

Following an 8-week period of standard growth, 12 WT mice and 12 Nogo-B$^{-/-}$ mice were randomly divided into the normal chow diet (NCD) or high-fat diet (HFD) groups, which were reared in a barrier system at temperatures ranging from 20 to 26 °C and fed either the NCD (SPF (Beijing) Biotechnology Co., Ltd.) or HFD (fat diet with 60 kcal%, MP Biomedicals, LLC) for 12 weeks. The specific composition of the HFD for mice is provided in supplementary material Table S2. Throughout the experiment, the weights of the mice were measured weekly. The animal experiment was approved by the Experimental Animal Welfare and Ethics Committee of the Fifth Medical Centre of the Chinese PLA General Hospital.

Glucose tolerance test (GTT) and insulin tolerance test (ITT)

At the beginning of week 11 of the experimental cycle, the mice in each group, which had fasted for 12 h, were intraperitoneally injected with the glucose solution at a dose of 2 g/kg body weight, and the tail vein blood glucose concentration was measured at 0, 15, 30, 60, 90, and 120 min using a Roche Diabetes Care glucometer. At the start of week 12, the blood glucose concentration was measured in the same method after intraperitoneal injection of 1 U/kg insulin (MedChemExpress (Monmouth Junction, NJ, USA)) solution into mice that had fasted for 4 h.

Sample acquisition

After the 12-week experiment, the overnight fasted mice were anesthetized with 3% sodium pentobarbital. Whole blood, liver, intestinal contents, and bone marrow-derived macrophages were then collected from the mice. The intestinal contents are extracted from the cecum to obtain sterile contents. The intestinal contents and a portion of the liver were immediately stored at -80 °C, while a portion of the liver tissue was immersed in 10% formalin for subsequent histological evaluation. The serum was recovered via centrifugation at 3000 rpm for 15 min at room temperature and then stored at −80 °C in endotoxin-free tubes until assayed. BMDMs were used for subsequent cell culture.

Cell culture

BMDMs were isolated from the femurs of model and control mice at the end of modeling, cultured in Dulbecco's modified Eagle's medium (DMEM; BOSTER, Wuhan, China) supplemented with 10% fetal bovine serum (FBS; VivaCell, Shanghai, China), 1% penicillin–streptomycin (MacGene), and 50 ng/ml mouse macrophage colony–stimulating factor (M-CSF, HY-P7085, MedChemExpress), and stimulated for 5 days in a cell culture chamber after differentiation.

Biochemical index detection

Serum biochemical indices included triacylglycerol (TG), total cholesterol (TC), low-density lipoprotein cholesterol (LDL-C), high-density lipoprotein cholesterol (HDL-C), alanine aminotransferase (ALT), aspartate aminotransferase (AST), alkaline phosphatase (ALP), and albumin (ALB), all of which were tested with commercial kits supplied by the Jiancheng Bioengineering Institute (Nanjing, China).

Histological evaluation

To evaluate the histological characteristics of the liver, such as lipid accumulation, inflammation, and fibrosis, liver tissues were fixed in 4% paraformaldehyde, embedded, sectioned, and mounted on microscope slides. Besides, a part of the fixed liver tissue was paraffin-embedded to obtain paraffin sections for hematoxylin and eosin (H&E) staining, and the other part was OCT-embedded to obtain frozen sections for oil red O staining. All images were captured with a Pannoramic MIDI scanner. Histological features were quantitatively assessed by ImageJ software (National Institutes of Health).

Western blot (WB) analysis

Total proteins from liver tissues were extracted using RIPA lysis buffer containing a phosphatase inhibitor, separated via 10% sodium dodecyl sulfate–polyacrylamide gel electrophoresis (SDS–PAGE), and transferred onto polyvinylidene fluoride (PVDF, Millipore, MA, USA) membranes. The membranes were blocked with TBST (GenStar, CA, USA) containing 5% fat-free milk for 1 h at room temperature and then incubated overnight with primary antibodies in TBST with 5% bovine serum albumin at 4 °C. After washing with TBST for 3×5 min, the membranes were incubated with horseradish peroxidase-conjugated secondary antibodies in TBST containing 5% fat-free milk for 1 h at room temperature. Protein expression levels on the PVDF membranes were detected utilizing the enhanced chemiluminescence (ECL) reagent (Promega, Beijing, China).

Quantitative real-time polymerase chain reaction (qRT–PCR)

Total RNA was isolated from liver tissue with TRIzol reagent, followed by reverse transcription into cDNA via StarScript III All-in-one RT Mix with gDNA Remover (Vazyme, Nanjing, China). Finally, the RNA levels were quantified using 2×Taq Pro Universal SYBR qPCR Master Mix (Vazyme, Nanjing, China) on a QuantStudio(TM) 6 Flex System. The amplification conditions included predenaturation at 95 °C for 30 s, followed by 40 cycles at 95 °C for 10 s, 60 °C for 30 s, and 95 °C for 15 s. Additionally, β-actin was used as an internal control to correct for RNA expression. The primers listed in supplementary

material Table S3 were synthesized by TIANYIHUIYUAN (Beijing, China).

ELISA

The cytokines TNF-α (tumor necrosis factor-alpha) and IL-6 (interleukin-6) in the liver were assayed using ELISA kits (Dakewe, Beijing, China) according to the manufacturer's instructions. Liver tissue samples of 50 mg were accurately weighed, 1 ml of PBS (PH 7.4) and 10 μL of protease inhibitor were added, then mechanically homogenized in an ice water bath and centrifuged at 3000 RPM for 20 min. Subsequently, the supernatant was carefully collected and the protein was quantified for detection and analysis. Cytokine levels are reported in pg/mg protein.

Gut microbiota (GM) analysis

Bioinformatics analysis of 16 S rRNA sequencing data was conducted using QIIME2 (version 1.9.1, http://qiime.org/install/index.html). Operational taxa (OTUs) with sequence homology and species taxonomic analysis ≥ 97% were clustered using UPARSE software (version 11, http://drive5.com/uparse/). Alpha diversity analysis was used to evaluate community richness and diversity, while principal component analysis (PCA) and principal coordinate analysis (PCoA) were used to assess structural alterations. The Wilcoxon rank-sum test was used to compare the levels of abundant taxa at the phylum and genus levels between the two groups. Finally, the correlations between biochemical indices or metabolites and the GM were measured using Spearman's analysis. The analysis was performed using the Majorbio Cloud online platform (https://cloud.majorbio.com).

UHPLC–MS analysis

The serum from five mice in each group was analyzed via UHPLC-Q-Orbitrap/MS. A quality control sample (QC) was created by combining equal volumes of all samples for system conditioning and quality control purposes. The QC samples were subjected to the same processing and testing procedures as the analytical samples. QC samples and blank samples (75% acetonitrile solution) were injected every 5 samples during collection. PCA, partial least squares discriminant analysis (PLS-DA), and orthogonal PLS-DA (OPLS-DA) were used to screen out the different variances between groups after scaling all metabolite variables to unit variance. Groups with variable importance in the projection (VIP) values > 1 and p values < 0.05 were statistically significant. The differential metabolites were identified by comparing typical and accurate quality MS/MS fragments with the Human Metabolome Database (HMDB, http://www.hmdb.ca) and then using the online database KEGG (http://www.kegg.jp) to screen the metabolic pathways for these metabolites. The results were analyzed via the Majorbio Cloud online platform (https://cloud.majorbio.com).

Statistical analysis

Continuous data were expressed as the means ± standard deviations (SDs) and were compared via the unpaired Student's t tests for two samples or two-way analysis of variance (ANOVA) for multiple samples. Then, Sidak's test or the Tukey–Kramer test was employed for multiple comparisons after ANOVA. All the statistical analyses and charts were completed with GraphPad Prism (version 8.0.2, https://www.graphpad.com/). A two-tailed p value < 0.05 was considered statistically significant.

Results

Nogo-B deficiency alleviates weight gain and impaired glucose tolerance in NAFLD model mice

After 12 weeks of modeling, the body and liver sizes of both the WT and KO mice were visually larger in the HFD group than in the NCD group. However, the body and liver sizes in the Nogo-B$^{-/-}$-HFD group were macroscopically smaller than those in the WT-HFD group. Interestingly, the liver had a visibly yellower color in the WT-HFD group than in the other groups (Fig. 2, A).

The body weights of the mice in each group were recorded weekly. The results showed that after knockdown of the Nogo-B gene, the mice exhibited a more significant difference in weight compared with the mice in the WT-HFD group. The difference in body weight between the two groups was statistically significant ($P < 0.05$) at all time points starting from two weeks after the treatment (Fig. 2, B). Moreover, the final body weights and liver weights of the two groups were also significantly different. ($P < 0.05$) (Fig. 2, C and D).

The GTT results revealed significantly greater blood glucose concentrations in the WT-HFD group than in the Nogo-B$^{-/-}$-HFD group at 30, 60, 90, and 120 min after glucose injection ($P < 0.05$) (Fig. 2, E). Moreover, the statistical analysis of the area under the curve (AUC) revealed that the AUC was greater for the HFD groups than for the NCD groups, whereas it was significantly smaller for the Nogo-B$^{-/-}$-HFD group than for the WT-HFD group ($P < 0.05$) (Fig. 2, F). However, the above phenomenon was not observed in the ITT experiment (Fig. 2, G and H).

Successful deletion of the Nogo-B protein in Nogo-B$^{-/-}$ mice was subsequently confirmed via WB analysis of mouse bone marrow-derived macrophages (BMDMs) (Fig. 2, I). Furthermore, WB analysis demonstrated that HFD feeding promoted Nogo-B protein expression in the liver tissue of WT mice (Fig. 2, J).

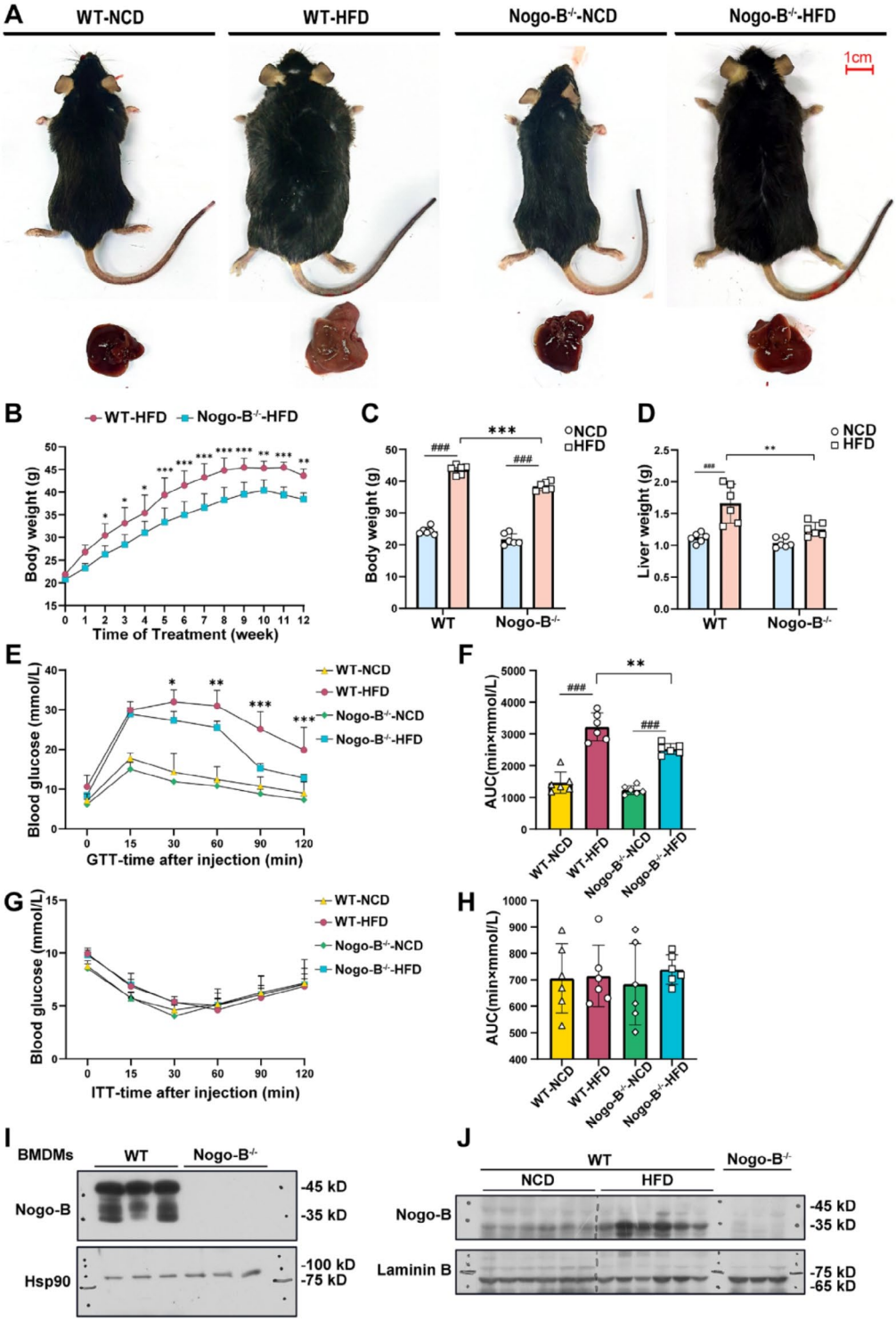

Fig. 2 Nogo-B deficiency alleviates weight gain and impaired glucose tolerance in NAFLD model mice. (**A**) Photos of the mice and their livers at the end of the 12-week experiment; (**B**) body weight (weekly); (**C**) body weight (last measurement); (**D**) liver weight (last measurement); (**E**) glucose tolerance test (GTT); (**F**) AUC of the GTT; (**G**) insulin tolerance test (ITT); (**H**) AUC of the ITT. $n = 6$. $^{\#}P < 0.05$, $^{\#\#}P < 0.01$, $^{\#\#\#}P < 0.001$; $^{*}P < 0.05$, $^{**}P < 0.01$, $^{***}P < 0.001$. NCD, normal chow diet; HFD, high-fat diet; AUC, area under the curve; BMDMs, bone marrow-derived macrophages; WT, wild-type; NCD, normal chow diet; HFD, high-fat diet

Nogo-B deficiency mitigates liver lipid accumulation and liver injury in NAFLD model mice

The serum biochemical indices of the mice were examined, revealing that a high-fat diet could cause abnormal blood lipids and liver function. In addition, the serum levels of TG, LDL-C, ALT, AST, and ALP were significantly lower in the Nogo-B$^{-/-}$-HFD group than in the WT-HFD group, whereas the levels of ALB were significantly higher ($P<0.05$). Curiously, HDL-C levels in the Nogo-B$^{-/-}$HFD group also decreased with Nogo-B deficiency ($P<0.05$). (Fig. 3, A-H)

H&E-stained sections revealed the absence of lipid accumulation in the livers of the NCD-fed mice, whereas cytoplasmic spherical lipid droplets of various sizes were observed in the HFD-fed mice. In the WT-HFD group, large lipid droplets filled more of the liver cytoplasm, pushing the nucleus to one side and possibly occupying the whole cell, which was attenuated by Nogo-B deficiency (Fig. 3, I). The sections stained with oil red O in each group exhibited an identical distribution of lipid droplets, and the quantitative analysis revealed that the relative area of lipid droplets in the Nogo-B$^{-/-}$-HFD group was significantly smaller than that in the WT-HFD group ($P<0.05$) (Fig. 3, J).

Nogo-B deficiency attenuates inflammation in the livers of NAFLD model mice

To determine the role of the Nogo-B protein in the liver, we examined the expression of inflammatory factors and macrophage surface markers. ELISA analysis revealed that HFD feeding upregulated the expression of TNF-α and IL-6 in the liver, whereas the lack of Nogo-B mitigated this upregulation, demonstrating a statistically significant difference ($P<0.05$) (Fig. 4A-B). The qRT−PCR results revealed a similar pattern to that observed for TNF-α and monocyte chemoattractant protein-1 (MCP-1) (Fig. 4, C−D).

Moreover, qRT−PCR analysis revealed a significant increase in the mRNA expression of M1 macrophage (M1) surface markers (CD80 and CD86) and M2 macrophage (M2) surface markers [Arg1 (arginase-1), Mgl2 (macrophage galactose N-acetyl-galactosamine specific lectin-2) and Retlna (resistin-like alpha), $P<0.05$]. Compared with WT-HFD-fed mice, Nogo-B$^{-/-}$-HFD-fed mice presented significantly decreased expression of CD80 and CD86 ($P<0.05$). In contrast, Nogo-B$^{-/-}$ mice presented increased expression of Arg1, Mgl2 and Retlna compared with WT mice in response to a HFD ($P<0.05$) (Fig. 4, E-I).

Nogo-B deficiency alters the GM in NAFLD model mice

The effects of Nogo-B on the GM were investigated via 16 S rRNA sequencing analysis of the intestinal contents of mice. The coverage index of the operational taxonomic unit (OTU) level was >99%. Alpha diversity analysis was used to evaluate the community's richness and diversity. First, the community richness of the GM in the Nogo-B$^{-/-}$-HFD group was greater than that in the WT-HFD group, as shown by the ACE and Chao indices, but the difference was not significant ($P>0.05$) (Fig. 5A and B). Compared with the WT-HFD group, the Nogo-B$^{-/-}$-HFD group presented greater community diversity, as evidenced by increased Shannon indices and decreased Simpson indices ($P<0.05$) (Fig. 5, C and D). Beta diversity analysis of the structure of the GM was then performed, and both PCA and PCoA, which were based on the Bray–Curtis distance, revealed distinct clustering in terms of microbiota composition between the Nogo-B$^{-/-}$-HFD and WT-HFD groups (Fig. 5, E and F).

According to the community histogram at the phylum level, *Firmicutes*, *Desulfobacterota*, *Bacteroidota*, *Verrucomicrobiota*, and *Proteobacteria* were the most abundant phyla in the two groups. Importantly, Nogo-B deficiency significantly reduced the *Firmicutes/Bacteroidetes* ratio (F/B, WT-HFD group 27.09 vs. Nogo-B$^{-/-}$-HFD group 3.47), as well as the percentage of abundance of harmful bacteria such as *Proteobacteria* and *Desulfobacterota*, and increased the percentage of beneficial bacteria such as *Verrucomicrobiota* and *Actinobacteria* (Fig. 5, G and H). At the genus level, *norank_f_Desulfovibrionaceae*, *Lachnospiraceae_NK4A136_group*, *Lactobacillus*, *unclassified_f_Lachnospiraceae*, and *Akkermansia* accounted for a large proportion of the abundance in the two groups. Moreover, compared with the WT-HFD group, the Nogo-B$^{-/-}$-HFD group presented greater abundances of *unclassified_f_Lachnospiraceae* and *Akkermansia*, and *norank_f__Muribaculaceae*, whereas the abundances of *norank_f_Desulfovibrionaceae*, *Lachnospiraceae_NK4A136_group*, and *Lactobacillus* were lower (Fig. 5, I).

To further explore the effect of the Nogo-B protein on the GM, we identified five genus-level communities that presented significant differences between the groups. The Nogo-B$^{-/-}$-HFD group showed a significant increase in these different communities (*Lachnoclostridium*, *Harryflintia*, *Odoribacter*, *UCG-009*, and *unclassified_f_Butyricicoccaceae*) ($P>0.05$) (Fig. 5, J-O).

Nogo-B deficiency regulates serum metabolites in NAFLD model mice

During the analysis process, we tested the aggregation state of the QC samples to ensure the reliability and stability of the experiment, and then the PCA model was applied on the two groups of datasets. The PCA score plot revealed a segregation tendency between the samples from the WT-HFD and the Nogo-B$^{-/-}$-HFD groups, indicating that the absence of Nogo-B could modulate the metabolic network of HFD-fed mice (Fig. 6, A).

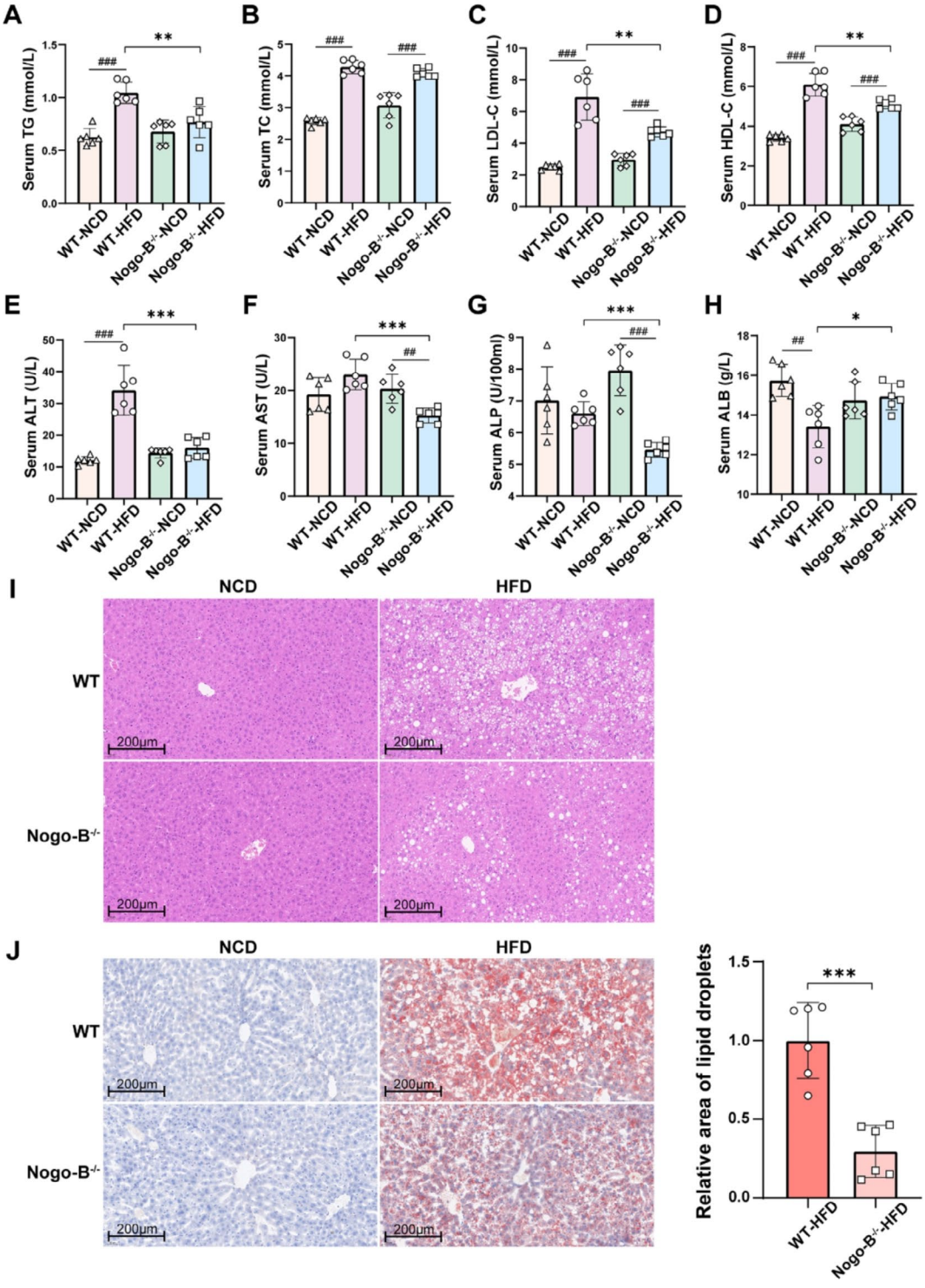

Fig. 3 Nogo-B deficiency mitigates liver lipid accumulation and liver injury in NAFLD model mice. (**A**) Serum triacylglycerol (TG); (**B**) serum total cholesterol (TC); (**C**) serum low-density lipoprotein cholesterol (LDL-C); (**D**) serum high-density lipoprotein cholesterol (HDL-C); (**E**) serum alanine aminotransferase (ALT); (**F**) serum aspartate aminotransferase (AST); (**G**) serum alkaline phosphatase (ALP); (**H**) serum albumin (ALB); (**I**) hematoxylin and eosin (**H**&**E**) staining of liver sections (scale bar: 200 μm); (**J**) oil red O staining of liver sections (scale bar: 200 μm). $n = 6$. $^{\#}P < 0.05$, $^{\#\#}P < 0.01$, $^{\#\#\#}P < 0.001$; $^{*}P < 0.05$, $^{**}P < 0.01$, $^{***}P < 0.001$. WT, wild-type; NCD, normal chow diet; HFD, high-fat diet

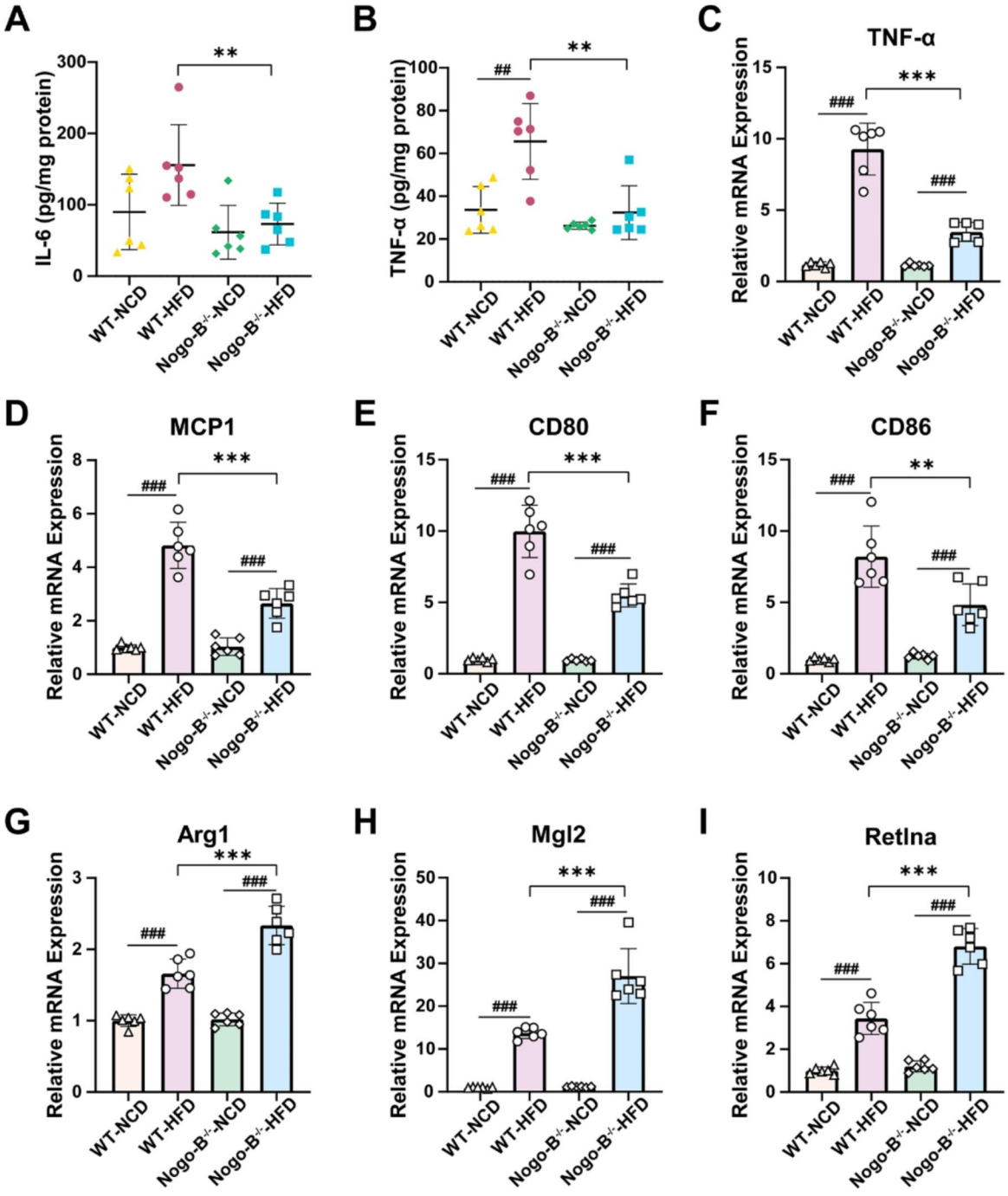

Fig. 4 Nogo-B deficiency attenuates inflammation in the livers of NAFLD model mice. (**A**) The concentration of interleukin-6 (IL-6); (**B**) the concentration of tumor necrosis factor-α (TNF-α); (**C**) the mRNA expression of tumor necrosis factor-α (TNF-α); (**D**) the mRNA expression of monocyte chemoattractant protein-1 (MCP1); (**E**) the mRNA expression of CD80; (**F**) the mRNA expression of CD86; (**G**) the mRNA expression of arginase-1 (Arg1); (**H**) the mRNA expression of arginase-1 (Arg1); (**I**) the mRNA expression of macrophage galactose N-acetyl-galactosamine specific lectin-2 (Mgl2); (**J**) the mRNA expression of resistin-like alpha (Retlna). $n = 6$. $^{\#}P < 0.05$, $^{\#\#}P < 0.01$, $^{\#\#\#}P < 0.001$; $^{*}P < 0.05$, $^{**}P < 0.01$, $^{***}P < 0.001$. WT, wild-type; NCD, normal chow diet; HFD, high-fat diet

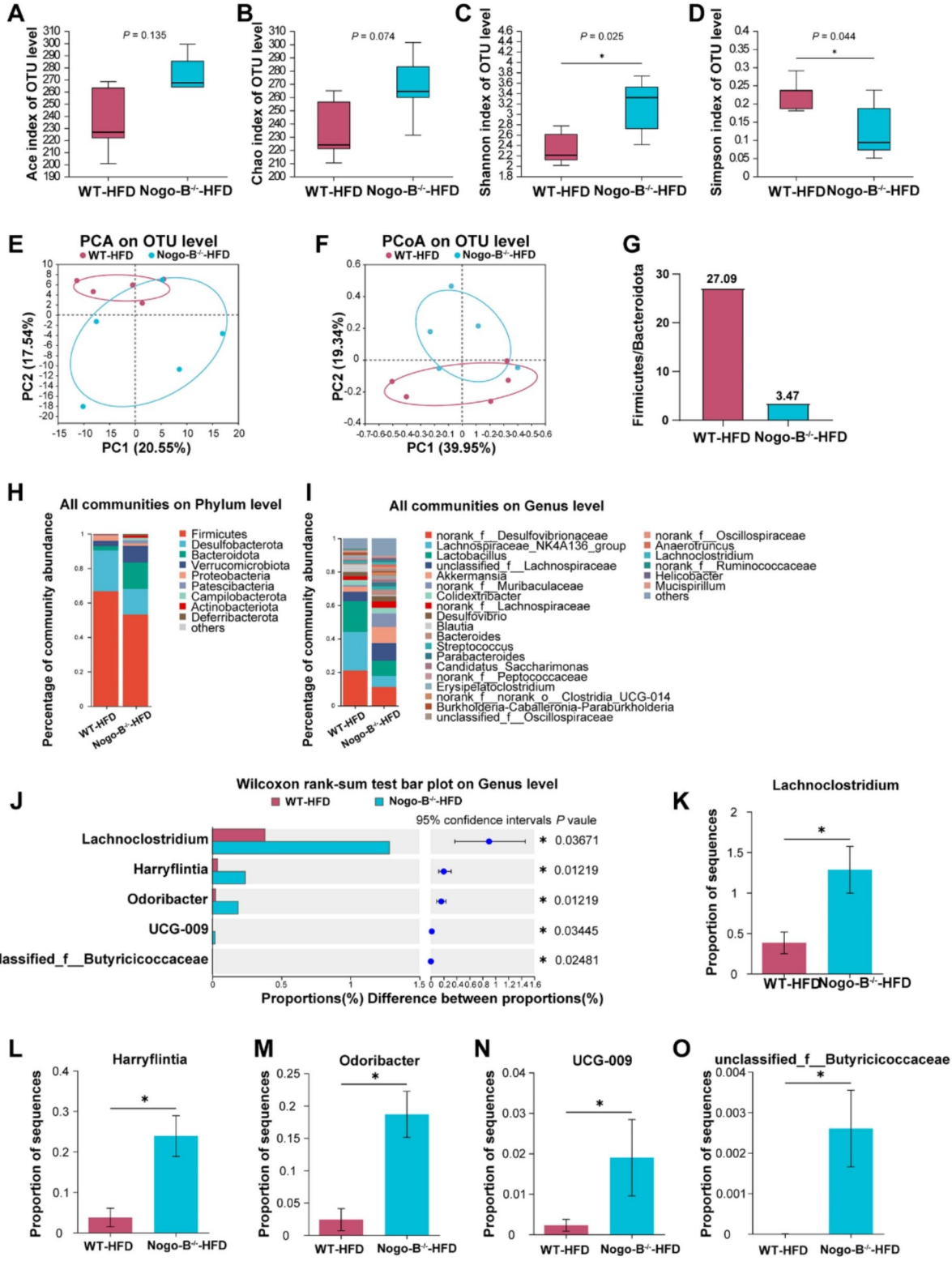

Fig. 5 (See legend on next page.)

(See figure on previous page.)

Fig. 5 Nogo-B deficiency alters the gut microbiota in NAFLD model mice. (**A**) Ace index; (**B**) Chao index; (**C**) Shannon index; (**D**) Simpson index; (**E**) principal component analysis (PCA); (**F**) principal coordinate analysis (PCoA); (**G**) Firmicutes/Bacteroidota (F/B) ratio; (**H**) percentage of all community abundances at the phylum level; (**I**) percentage of all community abundances at the genus level; (**J**) differential communities at the genus level selected by the Wilcoxon rank-sum test; (**K**) comparison of sequence proportions of *Lachnoclostridium* between groups; (**L**) comparison of sequence proportions of *Harryflintia* between groups; (**M**) comparison of sequence proportions of *Odoribacter* between groups; (**N**) comparison of sequence proportions of *UCG-009* between groups; (**O**) comparison of sequence proportions of *unclassified_f__Butyricicoccaceae* between groups; $n = 5$. $^{*}P < 0.05$, $^{**}P < 0.01$, $^{***}P < 0.001$. WT, wild-type; NCD, normal chow diet; HFD, high-fat diet; OTUs, operational taxonomic units

Supervised PLS-DA and OPLS-DA models were constructed to further discriminate the varying metabolites between the two groups, and separated clusters were examined between the metabolite profiles of the groups (Fig. 6, B and C). A permutation test of the OPLS-DA model was then conducted to verify the accuracy of the model, and the R2 parameter [R2=(0, 0.962)] and the Q2 parameter [Q2=(0, 0.01)] both revealed that the model could meet the predictive capacity of the data matrix (Fig. 6, D).

Additionally, the distinguishing metabolites between the Nogo-$B^{-/-}$-HFD and WT-HFD groups were screened out using the *P* values and VIP values of the OPLS-DA models, which were visualized using a volcano plot (Fig. 6, E). A total of 159 critical distinguishing metabolites were identified between the groups ($P<0.05$ and VIP > 1), and there were 79 significantly upregulated and 80 significantly downregulated metabolites in the Nogo-$B^{-/-}$-HFD group compared with the WT-HFD group. Moreover, the key differentially abundant metabolites with the top 30 VIP values are shown in Fig. 6F. Notably, in contrast to those in the WT-HFD group, metabolites such as uric acid, xanthosine, inosine, hypoxanthine, 10,11-dihydro-20-trihydroxy-leukotriene B4, prostaglandin E1, and taurodeoxycholic acid were upregulated after Nogo-B deficiency, whereas corticosterone, 13,14-dihydro-15-keto-pGE2, glycerol 3-phosphate, citric acid and isocitrate were downregulated.

To clarify the role of the Nogo-B protein in metabolism, pathway enrichment analysis was performed using the KEGG online database to explore the most relevant differentially abundant metabolite pathways and potential underlying mechanisms. KEGG pathways with the top 20 enrichment ratios of differential metabolites are shown in Fig. 6G.

Correlation analysis of the gut microbiota with serum biochemical indices and differentially abundant metabolites

To further determine the variation in the composition of the GM mediated by Nogo-B deficiency, Spearman correlation analyses were conducted between the gut communities and the serum biochemical parameters. At the phylum level, *Firmicutes* was negatively correlated with ALB, and *Bacteroidota* was negatively correlated with TG and AST ($P<0.05$) (Fig. 7, A). Moreover, TC was negatively correlated with *Actinobacteria* and positively associated with *Deferribacterota* ($P<0.05$) (Fig. 7, A). With respect to the genus-level differential communities, *Odoribacter*, *Harryflintia*, *unclassified_f__Butyricicoccaceae*, *Lachnoclostridium*, and *UCG-009* were negatively correlated with TG, LDL-C, HDL-C, ALT, AST, and ALP (Fig. 7, B). Notably, there was a significant positive correlation between *Odoribacter* and ALB, while this positive correlation was not significant in the other four differential communities (Fig. 7, B). Similarly, we conducted Spearman correlation analysis to explore the relationships between differential GM and metabolites (top 30 VIP values), and the results revealed that upregulated differentially abundant metabolites due to Nogo-B deficiency were positively correlated with differential communities at the genus level, whereas downregulated differential metabolites were negatively correlated with these communities (Fig. 7, C).

Discussion

It is not fully understood how Nogo-B affects the progression of NAFLD and its relationship with the gut microbiota and metabolites. To clarify this unresolved field, we conducted a multiomics analysis using HFD-fed Nogo-B knockout mice to examine the impact of Nogo-B on the GM and metabolites in NAFLD. In particular, we revealed that Nogo-B deficiency could delay the progression of NAFLD by regulating intestinal ecological disorders and metabolites and that Odorobacteria might play a considerable role in this process.

Li J et al. reported that Nogo-B expression was increased during white adipogenesis along with the upregulation of adipogenic markers, whereas Nogo-B deficiency inhibited the expression of white adipocyte markers and lipid accumulation via the AKT2/GSK3β/β-catenin pathway [23]. In addition, Nogo-B, as a metabolic regulator that is highly expressed in mouse and human NAFLD-associated HCC, accelerates metabolic dysfunction and tumorgenicity induced by a high-fat and high-carbohydrate diet; thus, inhibiting Nogo-B has a protective effect on metabolic syndrome [20, 24]. Consistently, in our study, the body and liver weights of Nogo-B-deficient model mice were significantly lower than those of NAFLD model mice, and histological evidence revealed that Nogo-B reduced lipid accumulation in hepatocytes. Hence, Nogo-B could improve obesity and reduce lipid accumulation in hepatocytes.

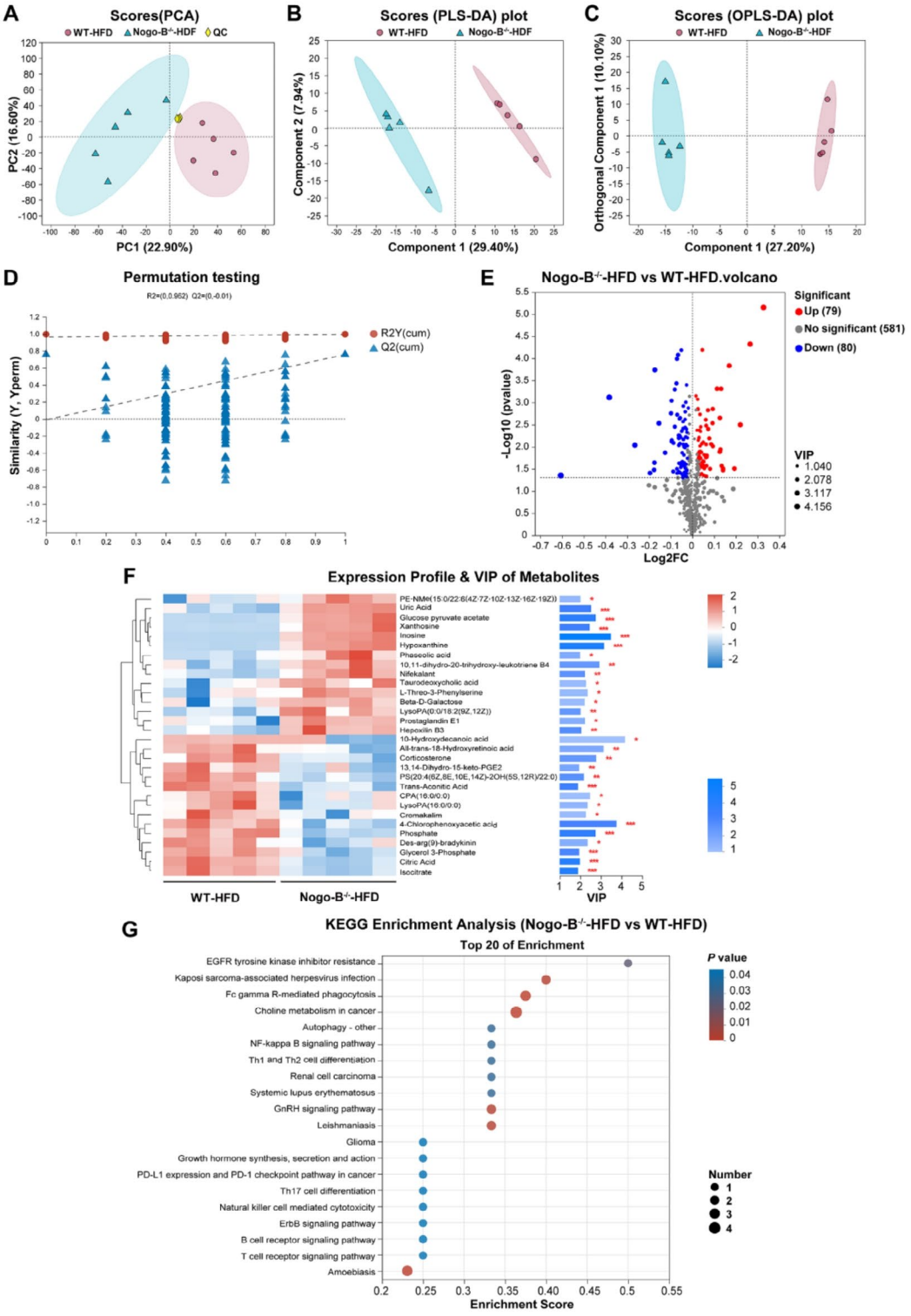

Fig. 6 Nogo-B deficiency regulates serum metabolites in NAFLD model mice. (**A**) Principal component analysis (PCA) score plot; (**B**) partial least squares discriminant analysis (PLS-DA) score plot; (**C**) orthogonal partial least squares discriminant analysis (OPLS-DA) score plot; (**D**) OPLS-DA permutation test; (**E**) volcano plot, in which the red spots represent the significantly upregulated metabolites (log2FC > 0), the blue spots represent the significantly downregulated metabolites (log2FC < 0), and the gray spots represent the nonsignificant metabolites ($P > 0.05$); (**F**) clustered heatmap and VIP value bar graphs of differentially abundant metabolites (top 30 VIP values) between the WT-HFD and Nogo-B$^{-/-}$-HDF groups; (**G**) KEGG pathways (top 20 enrichment ratios) of differentially abundant metabolites. $n = 5$. VIP, variable importance in the projection; WT, wild-type mice; NCD, normal chow diet; HFD, high-fat diet

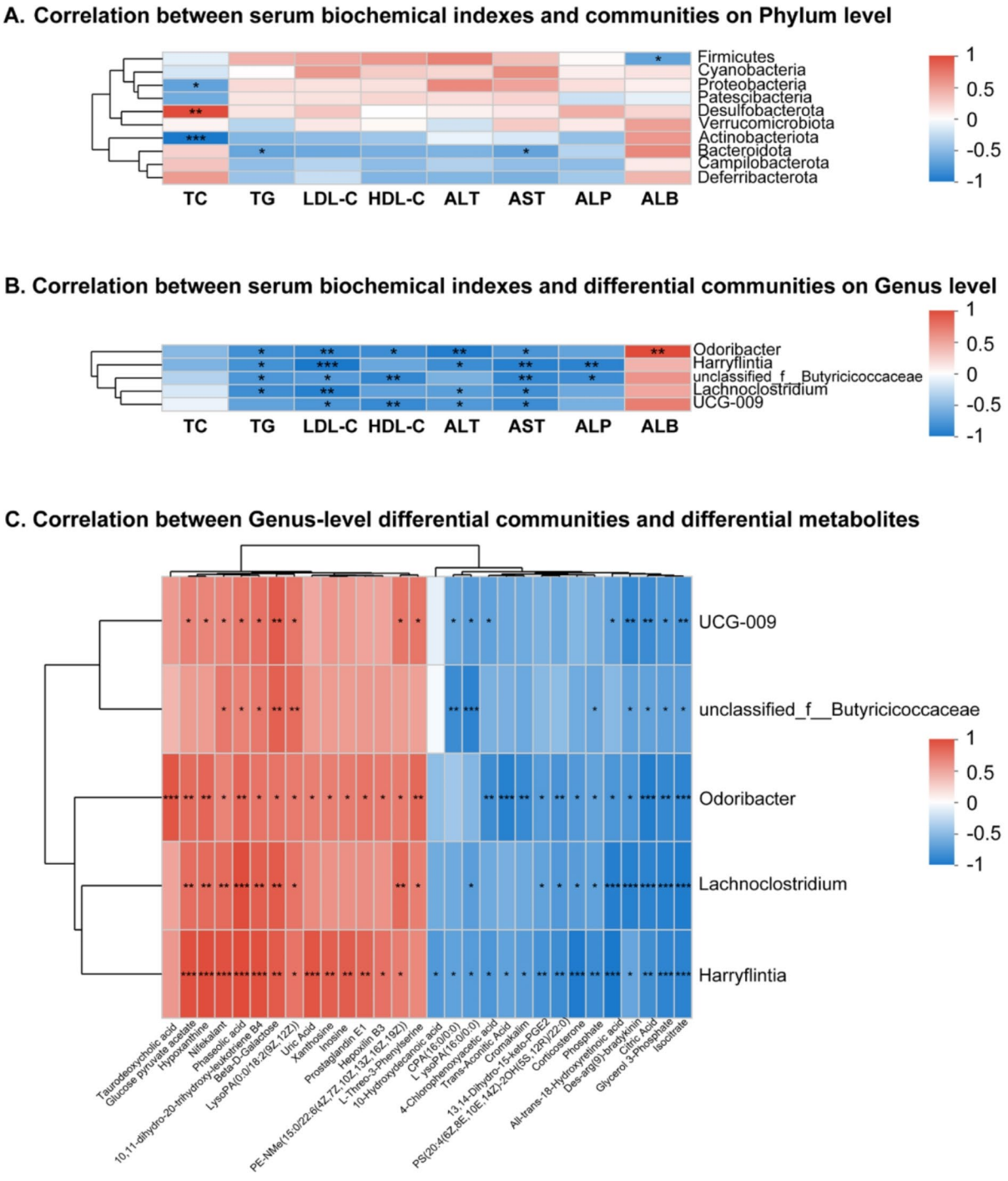

Fig. 7 Correlation analysis of the gut microbiota with serum biochemical indices and differentially abundant metabolites. (**A**) Correlations between serum biochemical indices and communities at the phylum level; (**B**) correlations between serum biochemical indices and differential communities at the genus level; (**C**) correlations between genus-level differential communities and differentially abundant metabolites. *$P < 0.05$, **$P < 0.01$, ***$P < 0.001$. TC, total cholesterol; TG triacylglycerol; LDL-C, low-density lipoprotein cholesterol; HDL-C, high-density lipoprotein cholesterol; ALT, alanine aminotransferase; AST, aspartate aminotransferase; ALP, alkaline phosphatase; ALB, albumin

Metabolic disorders are closely linked to the progression of NAFLD. Obesity, lipid abnormalities, and type 2 diabetes are independently associated with severe liver disease, with type 2 diabetes increasing the risk of advanced fibrosis, cirrhosis-related complications, and liver disease mortality by more than twofold [25]. Animal models have indicated that high-fat diets lead to peripheral insulin resistance and impaired glucose tolerance, followed by metabolic disorders such as hyperglycemia and hyperinsulinemia [26, 27]. Nogo-B is an important mediator of ChREBP activity and insulin sensitivity, and its deficiency improves insulin sensitivity, decreases the expression of ChREBP and lipogenesis molecules, and reduces endoplasmic reticulum stress and inflammation, thereby blocking high-glucose or high-fructose diet-induced hepatic lipid accumulation, impaired glucose tolerance, and other metabolic disorders [28]. Similarly, in our study, HFD-fed NAFLD model mice presented increased Nogo-B expression along with elevated postprandial blood glucose levels, indicating impaired glucose tolerance, which was ameliorated by Nogo-B deficiency. Moreover, Nogo-B deficiency also reversed the dyslipidemia (elevated TG, LDL-C, and HDL-C) caused by a HFD. Notably, HDL-C, a vascular lipid scavenger [29], also decreased with Nogo-B deficiency, suggesting that the absence of Nogo-B may reduce the deposition of lipids such as cholesterol transported by HDL in hepatocytes. In addition, McCullough A et al. reported that HDL-C levels are increased in patients with NAFLD [30]. In summary, Nogo-B deficiency ameliorates metabolic disorders such as lipid disturbance and impaired glucose tolerance in NAFLD.

Nogo-B plays a crucial role in regulating inflammatory factors during NAFLD progression. Kupffer cells (KCs), as hepatic resident macrophages, are important components of the innate immune system and play a role in clearance and phagocytosis in the liver [31]. When hepatocytes are injured, KCs respond first, leading to NF-κB activation, chemokine and pro-inflammatory cytokine (e.g., TNF-α, IL-1β and IL-6) induction, and monocyte recruitment [32]. The polarization of M1/M2 macrophages is closely associated with the progression of NAFLD [33]. An increase in M1-type KCs has been observed in patients with NASH [34]. Jianhua Rao et al. reported that Nogo-B deficiency reduces M1 macrophage polarization and inhibits the release of proinflammatory cytokines (e.g., TNF-α, IL-6, MCP-1, and iNOS) [35]. It has also been demonstrated that the presence of Nogo-B in mice results in increased hepatic steatosis and inflammation. Mechanistically, the increased ER stress within KCs caused by Nogo-B deficiency promotes M2 polarization and attenuates hepatic steatosis, inflammation, and injury [19]. In our study, Nogo-B deficiency decreased the release of inflammatory factors such as TNF-α, IL-6 and MCP-1 in KCs. Consistent with previous studies, Nogo-B deficiency inhibited M1 polarization, promoted M2 polarization, attenuated hepatic injury and inflammation, and delayed NAFLD progression, suggesting that Nogo-B may be a potential target for the treatment of NAFLD.

The bidirectional relationship between the GM and the liver, referred to as the gut–liver axis, is driven by a complicated interaction between liver injury, dysbiosis of the GM, intestinal barrier dysfunction, homeostasis imbalance of metabolites, and immune system dysregulation, contributing to the development of NAFLD [36]. Moreover, studies in animals and patients have shown that fatty diet-induced liver steatosis can disturb the balance of the intestinal environment [37–39]. The diversity of the intestinal community in NAFLD patients is significantly lower than that in healthy individuals, and the composition of the community is critically different [40, 41]. We found that Nogo-B deficiency apparently regulated the GM imbalance and increased the abundance and diversity of the community in NAFLD model mice. We demonstrated that Nogo-B deficiency decreased the F/B ratio, which is an important indicator of GM homeostasis and is elevated in patients with hyperlipidemia [42]. In addition, obesity and hyperlipidemia lead to an increase in harmful intestinal microbiota and a decrease in beneficial intestinal microbiota [13, 43, 44]. However, our study showed that Nogo-B deficiency reversed this phenomenon and increased the abundance of beneficial microbiota such as *Akkermansia*, which has shown a negative correlation with obesity and diabetes and other metabolic diseases [45, 46]. Therefore, it can be concluded that Nogo-B deficiency can improve the intestinal ecological disturbance caused by NAFLD.

Metabolites and their pathways influence the progression of NAFLD. The products of purine metabolism can inhibit the progression of NAFLD. Xanthosine mediates hepatic glucose homeostasis by regulating the AMPK/FoxO1/AKT/GSK3β signaling cascade to inhibit gluconeogenesis and to activate glycogenesis [47], and inosine significantly enhances β-oxidation and inhibits proinflammatory cytokine expression and hepatic pyrodeath [48]. Specifically, Nogo-B deletion upregulated the expression of purine metabolites in our study. Moreover, there is a strong correlation between gut microbes and bile acids in the host, and tauroursodeoxycholic acid has been reported to attenuate the progression of HFD-induced NAFLD in mice by improving intestinal inflammation, ameliorating intestinal barrier function, reducing intestinal fat transport, and modulating the intestinal microbiota composition [49, 50]. We found that Nogo-B deficiency upregulated the expression of taurodeoxycholic acid. In addition, corticosterone can lead to metabolic disorders such as severe insulin resistance,

hyperglycemia, and hypertriglyceridemia and even mediate the upregulation of liver CD36 to promote the occurrence of NAFLD [51, 52]. Moreover, metabolites of the tricarboxylic acid cycle are also involved in the occurrence of NAFLD [53], and circulating levels of isocitrate and citric acid are significantly increased in patients with NAFLD [54]. Importantly, our study revealed that Nogo-B deficiency downregulated the levels of corticosterone and metabolites of the tricarboxylic acid cycle. Thus, Nogo-B deficiency may delay the progression of NAFLD by regulating metabolites. Furthermore, we identified metabolic pathways with high enrichment rates through differentially abundant metabolites, indicating that Nogo-B is closely associated with pathways related to the progression of liver diseases, such as metabolic disorders (e.g., EGFR tyrosine kinase inhibitor resistance and autophagy), hepatic inflammation (e.g., the NF-κB signaling pathway), the immune response (e.g., the B-cell receptor signaling pathway, natural killer cell-mediated cytotoxicity and the T-cell receptor signaling pathway, and Fc γR-mediated phagocytosis), and the development of malignancy (e.g., choline metabolism in cancer and PD-L1 expression and the PD-1 checkpoint pathway in cancer).

Gut microbes interact with metabolites to promote the progression of NAFLD. Endotoxins/lipopolysaccharides derived from intestinal microbes activate KCs, leading to the secretion of proinflammatory cytokines that contribute to the development of NAFLD [55]. Transplanting the fecal microbiota from patients with NAFLD to recipient mice increases the accumulation and activation of B cells in the liver, resulting in hepatic inflammation and fibrosis in NASH [56]. Our study revealed that *Firmicutes* was negatively correlated with ALB, an indicator of liver synthetic function, whereas *Bacteroidota* was positively correlated with ALB. Moreover, the F/B ratio decreased following Nogo-B deficiency, indicating that intestinal microorganisms might regulate hepatic synthesis function and that Nogo-B deficiency might participate in this process. Furthermore, the various microbes screened in the HFD group with Nogo-B deficiency presented consistent associations with serum lipid and liver function indices, demonstrating that the remission of serum lipid increases and liver injury and the recovery of hepatic synthetic function might be related to the increased abundance of microorganisms after Nogo-B deficiency. In particular, *Odoribacter*, belonging to *Bacteroidota*, is a common short-chain fatty acid-producing member of the human GM, and its decreased abundance is associated with NAFLD [57]. In addition, as a probiotic with anti-inflammatory activity, *Odoribacter* can deplete succinic acid and mitigate inflammation related to glucose tolerance and obesity [58]. In terms of the associations between intestinal microorganisms and metabolites, the differential microorganisms were positively correlated with the upregulated purine metabolism and bile acid metabolites associated with Nogo-B deficiency, whereas they were negatively correlated with the downregulated corticosterone and tricarboxylic acid cyclic metabolites associated with Nogo-B deficiency. These results revealed the interaction of Nogo-B proteins, differential microbes such as Odoribacter, and the abovementioned metabolic pathways. Accordingly, Nogo-B deficiency might increase beneficial bacteria, such as *Odoribacter*, and regulate corticosterone and the products of purine metabolism, bile acid metabolism, and the tricarboxylic acid cycle, delaying the progression of NAFLD. However, the causal relationships among these three factors need to be further verified due to the limitations of the experimental design.

In conclusion, Nogo-B deficiency can improve metabolic disorders, reduce hepatocellular lipid accumulation, alleviate inflammation and liver injury, and delay the progression of NAFLD in NAFLD model mice. This effect might be achieved by regulating intestinal ecological disorders and metabolites and their pathways, suggesting that Nogo-B could be a potential target for NAFLD treatment. Additionally, our study revealed a significant increase in the community abundance of *Odoribacter* after Nogo-B deficiency, which was strongly positively correlated with ALB and taurodeoxycholic acid. This discovery was novel, and we hypothesize that *Odoribacter* plays a meaningful role in Nogo-B to affect NAFLD progression.

Abbreviations

NAFLD	Nonalcoholic fatty liver disease
GM	Gut microbiota
HFD	High-fat diet
GTT	Glucose tolerance test
ITT	Insulin tolerance test
F/B	Firmicutes/Bacteroidota
KO	Knockout
WT	Wild-type mice
ALB	Albumin
HCC	Hepatocellular carcinoma
IR	Insulin resistance
NASH	Non-alcoholic steatohepatitis
ER	Endoplasmic reticulum
BMDMs	Bone marrow-derived macrophages
NCD	Normal chow diet
TG	Triacylglycerol
TC	Total cholesterol
LDL	C-Low-density lipoprotein cholesterol
HDL	C-High-density lipoprotein cholesterol
ALT	Alanine aminotransferase
AST	Aspartate aminotransferase
ALP	Alkaline phosphatase
H&E	Hematoxylin and eosin
WB	Western blotting analysis
qRT	PCR-Quantitative real-time polymerase chain reaction
TNF	a-Tumor necrosis factor-alpha
IL	6-Interleukin-6
PCA	Principal component analysis
PCoA	Principal coordinate analysis
QC	Quality control sample
PLS	DA-Partial least squares discriminant analysis

OPLS	DA-Orthogonal partial least squares discriminant analysis
VIP	Variable importance in the projection
MCP	1-Monocyte chemoattractant protein-1
M1	M1 macrophage
M2	M2 macrophage
Arg1	Arginase-1
Mgl2	Macrophage galactose N-acetyl-galactosamine specific lectin-2
Retlna	Resistin-like alpha
OTU	Operational taxonomic units
KCs	Kupffer cells

Supplementary Information

The online version contains supplementary material available at https://doi.org/10.1186/s12263-024-00754-5.

Supplementary Material 1

Author contributions

LLG, ZFB and XHX acquired funding for the study and supervised the project. In this study, XD, LLG and ZFB designed the experiments. XD performed most of the experiments, besides, XD, YTX and TTH analyzed the data. CYZ, JJL, YJZ, YJX, YX, ZXW and XMZ provided assistance with the investigation. LLG provided assistance with animal resources. XD and YTX wrote the original draft, and LLG, ZFB and XHX revised the manuscript.

Funding

This study was granted by the National Natural Science Foundation of China (Grant No. 81570563), the Natural Science Foundation of Beijing, China (Grant No. 7232321), Beijing Nova Program (Grant No. 20230484395), the Innovation Team and Talents Cultivation Program of National Administration of Traditional Chinese Medicine (No: ZYYCXTD-C-202005) and the Foundation for Innovative Research Groups of the National Natural ScienceFoundation of China (Grant No. 81721002).

Data availability

All data generated during and/or analyzed during the current study are available from the corresponding author upon reasonable request.

Declarations

Competing interests

The authors declare no competing interests.

Author details

[1]Medical School of Chinese PLA, Beijing, China
[2]Department of Gastroenterology, The Second Medical Center, Chinese PLA General Hospital, Beijing, China
[3]Department of Hepatology, The Fifth Medical Center, Chinese PLA General Hospital, Beijing, China
[4]307 Clinical Medical College of PLA, Anhui Medical University, Beijing, China
[5]Department of Hepatology Medicine of Traditional Chinese Medicine, The Fifth Medical Center, Chinese PLA General Hospital, Beijing, China
[6]China Military Institute of Chinese Materia, The Fifth Medical Center, Chinese PLA General Hospital, Beijing, China
[7]School of Chengde Medical University, Chengdeshi, China

Received: 12 January 2024 / Accepted: 11 August 2024
Published online: 24 August 2024

References

1. Haldar D, Kern B, Hodson J, et al. Outcomes of liver transplantation for non-alcoholic steatohepatitis: a European Liver Transplant Registry study. J Hepatol. 2019;71:313–22.
2. Riazi K, Azhari H, Charette JH, et al. The prevalence and incidence of NAFLD worldwide: a systematic review and meta-analysis. Lancet Gastroenterol Hepatol. 2022;7:851–61.
3. Powell EE, Wong VW-S, Rinella M. Non-alcoholic fatty liver disease. Lancet. 2021;397:2212–24.
4. Polyzos SA, Kountouras J, Mantzoros CS. Obesity and nonalcoholic fatty liver disease: from pathophysiology to therapeutics. Metab Clin Exp. 2019;92:82–97.
5. En Li Cho E, Ang CZ, Quek J, et al. Global prevalence of non-alcoholic fatty liver disease in type 2 diabetes mellitus: an updated systematic review and meta-analysis. Gut. 2023;72:2138–48.
6. Lomonaco R, Ortiz-Lopez C, Orsak B, et al. Effect of adipose tissue insulin resistance on metabolic parameters and liver histology in obese patients with nonalcoholic fatty liver disease. Hepatology. 2012;55:1389–97.
7. Sanyal AJ. Past, present and future perspectives in nonalcoholic fatty liver disease. Nat Rev Gastroenterol Hepatol. 2019;16:377–86.
8. Friedman SL, Neuschwander-Tetri BA, Rinella M, Sanyal AJ. Mechanisms of NAFLD development and therapeutic strategies. Nat Med. 2018;24:908–22.
9. Boursier J, Mueller O, Barret M, et al. The severity of nonalcoholic fatty liver disease is associated with gut dysbiosis and shift in the metabolic function of the gut microbiota. Hepatology. 2016;63:764–75.
10. Aron-Wisnewsky J, Warmbrunn MV, Nieuwdorp M, Clément K. Nonalcoholic fatty liver disease: modulating gut microbiota to Improve. Severity? Gastroenterol. 2020;158:1881–98.
11. Turnbaugh PJ, Hamady M, Yatsunenko T, et al. A core gut microbiome in obese and lean twins. Nature. 2009;457:480–4.
12. Loomba R, Seguritan V, Li W, et al. Gut microbiome-based metagenomic signature for non-invasive detection of Advanced Fibrosis in Human nonalcoholic fatty liver disease. Cell Metab. 2017;25:1054–e10625.
13. Caussy C, Tripathi A, Humphrey G, et al. A gut microbiome signature for cirrhosis due to nonalcoholic fatty liver disease. Nat Commun. 2019;10:1406.
14. Kakiyama G, Pandak WM, Gillevet PM, et al. Modulation of the fecal bile acid profile by gut microbiota in cirrhosis. J Hepatol. 2013;58:949–55.
15. Boghdadi AG, Teo L, Bourne JA. The involvement of the myelin-Associated inhibitors and their receptors in CNS plasticity and Injury. Mol Neurobiol. 2018;55:1831–46.
16. Schwab ME, Strittmatter SM. Nogo limits neural plasticity and recovery from injury. Curr Opin Neurobiol. 2014;27:53–60.
17. Schanda K, Hermann M, Stefanova N, Gredler V, Bandtlow C, Reindl M. Nogo-B is associated with cytoskeletal structures in human monocyte-derived macrophages. BMC Res Notes. 2011;4:6.
18. Zhao X, Wang X, You Y, et al. Nogo-B fosters HCC progression by enhancing Yap/Taz-mediated tumor-associated macrophages M2 polarization. Exp Cell Res. 2020;391:111979.
19. Park J-K, Shao M, Kim MY, et al. An endoplasmic reticulum protein, Nogo-B, facilitates alcoholic liver disease through regulation of kupffer cell polarization. Hepatology. 2017;65:1720–34.
20. Tian Y, Yang B, Qiu W, et al. ER-residential Nogo-B accelerates NAFLD-associated HCC mediated by metabolic reprogramming of oxLDL lipophagy. Nat Commun. 2019;10:3391.
21. Zhao D, Xue C, Yang Y, et al. Lack of Nogo-B expression ameliorates PPARγ deficiency-aggravated liver fibrosis by regulating TLR4-NF-κB-TNF-α axis and macrophage polarization. Biomed Pharmacother. 2022;153:113444.
22. Liu B, Zhuang Y, Dong X, Wang J, Gao L. Preparation of Nogo-B knockout mouse model by CRISPR/Cas9 technique. World Latest Med Inform. 2019;19:108–9.
23. Li J, Sun Y, Xue C, et al. Nogo-B deficiency suppresses white adipogenesis by regulating β-catenin signaling. Life Sci. 2023;321:121571.
24. Gong K, Zhang Z, Chen S-S, et al. 6-Methyl flavone inhibits Nogo-B expression and improves high fructose diet-induced liver injury in mice. Acta Pharmacol Sin July; 2023.
25. Jarvis H, Craig D, Barker R, et al. Metabolic risk factors and incident advanced liver disease in non-alcoholic fatty liver disease (NAFLD): a systematic review and meta-analysis of population-based observational studies. PLoS Med. 2020;17:e1003100.
26. Winzell MS, Ahrén B. The high-fat diet-fed mouse: a model for studying mechanisms and treatment of impaired glucose tolerance and type 2 diabetes. Diabetes. 2004;53(Suppl 3):S215–219.
27. Bernardi S, Toffoli B, Tisato V, et al. TRAIL reduces impaired glucose tolerance and NAFLD in the high-fat diet fed mouse. Clin Sci. 2018;132:69–83.

28. Zhang S, Guo F, Yu M, et al. Reduced nogo expression inhibits diet-induced metabolic disorders by regulating ChREBP and insulin activity. J Hepatol. 2020;73:1482–95.
29. Zanoni P, Khetarpal SA, Larach DB, et al. Rare variant in scavenger receptor BI raises HDL cholesterol and increases risk of coronary heart disease. Science. 2016;351:1166–71.
30. McCullough A, Previs SF, Dasarathy J, et al. HDL flux is higher in patients with nonalcoholic fatty liver disease. Am J Physiol Endocrinol Metab. 2019;317:E852–62.
31. Malhi H, Gores GJ. Molecular mechanisms of lipotoxicity in nonalcoholic fatty liver disease. Semin Liver Dis. 2008;28:360–9.
32. Tosello-Trampont A-C, Landes SG, Nguyen V, Novobrantseva TI, Hahn YS. Kupffer cells trigger nonalcoholic steatohepatitis development in diet-induced mouse model through tumor necrosis factor-α production. J Biol Chem. 2012;287:40161–72.
33. Su GL, Goyert SM, Fan M-H, et al. Activation of human and mouse kupffer cells by lipopolysaccharide is mediated by CD14. Am J Physiol Gastrointest Liver Physiol. 2002;283:G640–645.
34. Sica A, Mantovani A. Macrophage plasticity and polarization: in vivo veritas. J Clin Investig. 2012;122:787–95.
35. Rao J, Cheng F, Zhou H, et al. Nogo-B is a key mediator of hepatic ischemia and reperfusion injury. Redox Biol. 2020;37:101745.
36. Blesl A, Stadlbauer V. The gut-liver Axis in Cholestatic Liver diseases. Nutrients. 2021;13:1018.
37. Aron-Wisnewsky J, Vigliotti C, Witjes J, et al. Gut microbiota and human NAFLD: disentangling microbial signatures from metabolic disorders. Nat Rev Gastroenterol Hepatol. 2020;17:279–97.
38. Lee G, You HJ, Bajaj JS, et al. Distinct signatures of gut microbiome and metabolites associated with significant fibrosis in non-obese NAFLD. Nat Commun. 2020;11:4982.
39. Wang W, Xu AL, Li ZC, et al. Combination of Probiotics and Salvia Miltiorrhiza Polysaccharide alleviates hepatic steatosis via gut microbiota modulation and Insulin Resistance Improvement in High Fat-Induced NAFLD mice. Diabetes Metab J. 2020;44:336–48.
40. Wang B, Jiang X, Cao M, et al. Altered fecal microbiota correlates with liver biochemistry in nonobese patients with non-alcoholic fatty liver disease. Sci Rep. 2016;6:32002.
41. Hui D, Liu L, Azami NLB, et al. The spleen-strengthening and liver-draining herbal formula treatment of non-alcoholic fatty liver disease by regulation of intestinal flora in clinical trial. Front Endocrinol. 2022;13:1107071.
42. Ru Y, Chen X, Wang J, et al. Structural characterization, hypoglycemic effects and mechanism of a novel polysaccharide from Tetrastigma Hemsleyanum Diels et Gilg. Int J Biol Macromol. 2019;123:775–83.
43. Zhang L, Zi L, Kuang T, et al. Investigating causal associations among gut microbiota, metabolites, and liver diseases: a mendelian randomization study. Front Endocrinol. 2023;14:1159148.
44. Zhao D, Cao J, Jin H, Shan Y, Fang J, Liu F. Beneficial impacts of fermented celery (Apium graveolens L.) juice on obesity prevention and gut microbiota modulation in high-fat diet fed mice. Food Funct. 2021;12:9151–64.
45. Wu J, Wang K, Wang X, Pang Y, Jiang C. The role of the gut microbiome and its metabolites in metabolic diseases. Protein Cell. 2021;12:360–73.
46. Depommier C, Everard A, Druart C, et al. Supplementation with Akkermansia muciniphila in overweight and obese human volunteers: a proof-of-concept exploratory study. Nat Med. 2019;25:1096–103.
47. Ahmed SA, Sarma P, Barge SR, Swargiary D, Devi GS, Borah JC. Xanthosine, a purine glycoside mediates hepatic glucose homeostasis through inhibition of gluconeogenesis and activation of glycogenesis via regulating the AMPK/FoxO1/AKT/GSK3β signaling cascade. Chem Biol Interact. 2023;371:110347.
48. Qiu J, Chen L, Zhang L, et al. Xie Zhuo Tiao Zhi formula modulates intestinal microbiota and liver purine metabolism to suppress hepatic steatosis and pyroptosis in NAFLD therapy. Phytomedicine. 2023;121:155111.
49. Wang W, Zhao J, Gui W, et al. Tauroursodeoxycholic acid inhibits intestinal inflammation and barrier disruption in mice with non-alcoholic fatty liver disease. Br J Pharmacol. 2018;175:469–84.
50. Liu J, Sun J, Yu J, et al. Gut microbiome determines therapeutic effects of OCA on NAFLD by modulating bile acid metabolism. NPJ Biofilms Microbiomes. 2023;9:29.
51. Candia R, Riquelme A, Baudrand R, et al. Overexpression of 11β-hydroxysteroid dehydrogenase type 1 in visceral adipose tissue and portal hypercortisolism in non-alcoholic fatty liver disease. Liver Int. 2012;32:392–9.
52. Tsai S-F, Hung H-C, Shih MM-C, et al. High-fat diet-induced increases in glucocorticoids contribute to the development of non-alcoholic fatty liver disease in mice. FASEB J. 2022;36:e22130.
53. Iacobazzi V, Infantino V. Citrate–new functions for an old metabolite. Biol Chem. 2014;395:387–99.
54. Sandlers Y, Shah RR, Pearce RW, Dasarathy J, McCullough AJ, Dasarathy S. Plasma krebs cycle intermediates in nonalcoholic fatty liver disease. J Clin Med. 2020;9:314.
55. Albillos A, de Gottardi A, Rescigno M. The gut-liver axis in liver disease: pathophysiological basis for therapy. J Hepatol. 2020;72:558–77.
56. Barrow F, Khan S, Fredrickson G, et al. Microbiota-Driven activation of Intrahepatic B cells aggravates NASH through Innate and Adaptive Signaling. Hepatology. 2021;74:704–22.
57. Hiippala K, Barreto G, Burrello C, et al. Novel Odoribacter splanchnicus strain and its outer membrane vesicles exert Immunoregulatory effects in vitro. Front Microbiol. 2020;11:575455.
58. Huber-Ruano I, Calvo E, Mayneris-Perxachs J, et al. Orally administered Odoribacter laneus improves glucose control and inflammatory profile in obese mice by depleting circulating succinate. Microbiome. 2022;10:135.

Publisher's Note